Atmospheric Environment 318 (2024) 120248

Contents lists available at ScienceDirect

Atmospheric Environment

journal homepage: www.elsevier.com/locate/atmosenv

Effects of NO and SO_2 on the secondary organic aerosol formation from isoprene photooxidation

Zhaoyan Zhang [a,b], Yingqi Zhao [a,b], Ya Zhao [a], Xiangyu Zang [a], Hua Xie [a], Jiayue Yang [a], Weiqing Zhang [a], Guorong Wu [a], Gang Li [a,**], Xueming Yang [a,c,d], Ling Jiang [a,c,*]

[a] State Key Laboratory of Molecular Reaction Dynamics, Dalian Institute of Chemical Physics, Chinese Academy of Sciences, 457 Zhongshan Road, Dalian 116023, China
[b] University of Chinese Academy of Sciences, 19A Yuquan Road, Beijing 100049, China
[c] Hefei National Laboratory, Hefei 230088, China
[d] Department of Chemistry and Guangdong Provincial Key Laboratory of Catalytic Chemistry, Southern University of Science and Technology, Shenzhen 518055, China

HIGHLIGHTS

- The study investigates the atmospheric components affected by the anthropogenic-biogenic interactions.
- The accumulated O_3 upon the NO conversion triggers the isoprene oxidation.
- The presence of SO_2 accelerates the conversion of NO and the accumulation of O_3, which promotes the main oxidation reaction of isoprene.
- Newly-observed compounds measured by threshold photoionization advance understanding of atmospheric components.

GRAPHICAL ABSTRACT

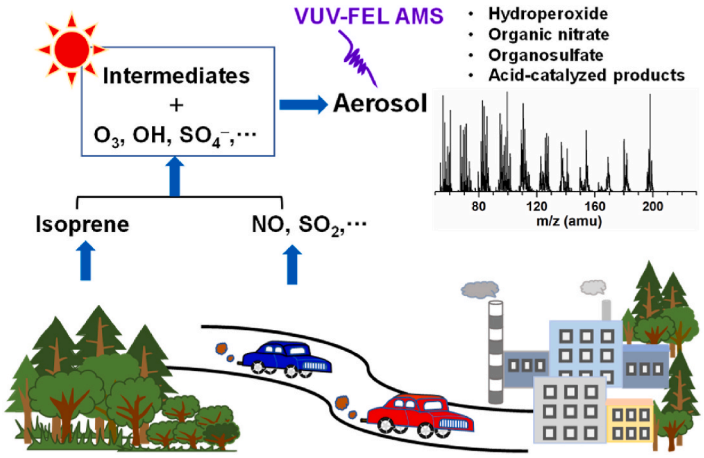

ARTICLE INFO

Keywords:
Atmospheric components
Volatile organic compound
Anthropogenic pollutant
Photooxidation
Reaction mechanism

ABSTRACT

Investigation of the effects of anthropogenic pollutants on the mass concentrations, particle number concentrations, and chemical compositions of secondary organic aerosol (SOA) formation is essential in understanding the photooxidation mechanism of volatile organic compounds but has been proven to be a very challenging experimental target because of their complex processes. Here, the effects of NO and SO_2 on SOA formation from isoprene photooxidation were studied by a number of laboratory studies. The results indicate the accumulated O_3 upon the NO conversion triggers the main oxidation reaction, by which the oxidants (i.e., OH and SO_4^-) are derived. The SOA mass concentrations and particle number concentrations are enhanced by NO under low NO

* Corresponding author. State Key Laboratory of Molecular Reaction Dynamics, Dalian Institute of Chemical Physics, Chinese Academy of Sciences, 457 Zhongshan Road, Dalian 116023, China.
** Corresponding author.
E-mail addresses: gli@dicp.ac.cn (G. Li), ljiang@dicp.ac.cn (L. Jiang).

https://doi.org/10.1016/j.atmosenv.2023.120248
Received 25 September 2023; Received in revised form 21 November 2023; Accepted 23 November 2023
Available online 28 November 2023

concentrations but suppressed by NO under high NO concentrations, which are consistent with previous studies (Kroll et al., 2005, 2006). This could be rationalized that the large amount of accumulated O_3 inhibit the multi-step isoprene oxidation and a large number of less oxidized products ($m/z < 130$) absorb or condense on the surface of existing particles, which decelerate the SOA nucleation and growth. The presence of SO_2 accelerates the conversion of NO and the accumulation of O_3, which promotes the main oxidation reaction of isoprene. New compounds are observed at $m/z = 134$, 137, 150, 152, and 179 measured by threshold photoionization (positive ion mode) with a tunable vacuum ultraviolet free electron laser and are found to be mainly formed from the isoprene oxidization by O_3 and OH. The present findings provide both macroscopic and microscopic information to advance understanding of atmospheric components affected by the anthropogenic-biogenic interactions in the neighborhood of emission origins.

1. Introduction

Isoprene is the most abundant non-methane volatile organic compound (VOC) in the atmosphere, with emissions estimated at 535 Tg/year (Guenther et al., 2012). As the isoprene possesses the structural peculiarity with two double bonds, its oxidation by the radicals and oxidants (i.e., OH, O_3, and NO_3) readily occurs in the atmosphere (Atkinson et al., 2006; Kwok et al., 1996; Ruppert and Becker, 2000; Wennberg et al., 2018; Zhao et al., 2021). Laboratory studies and field measurements indicated that the multi-generational oxidation products of isoprene can participate in the generation of particles through the formation of semi-volatility, low-volatility and extremely low-volatility organic compounds (SVOCs, LVOCs, ELVOCs), which significantly contribute to the source of secondary organic aerosol (SOA) (Bryant et al., 2020; Claeys et al., 2004; Dommen et al., 2006; Edney et al., 2005; Kroll et al., 2006; Lin et al., 2012; Surratt et al., 2006, 2010; Wennberg et al., 2018) and affect the SOA yields of other VOCs (Heinritzi et al., 2020; McFiggans et al., 2019). The reactive chemistry of isoprene influences the oxidation capacity of troposphere, the chemical cycle of nitrogen oxides, the Earth's radiative balance, and the human lung cells (Arashiro et al., 2016; Brauer et al., 2016; Eaves et al., 2020; Ehn et al., 2014; Hallquist et al., 2009; Kramer et al., 2016; Lelieveld et al., 2008; Lewis, 2018; Lin et al., 2016, 2017; Shiraiwa et al., 2017).

The studies on the effects of anthropogenic pollutants (i.e., NO_x, SO_2, etc.) on VOC photooxidation help to understand the initial steps of oxidation and the subsequent processes of new particle formation (Xu et al., 2015). Extensive efforts have been made for the isoprene oxidation at the molecular level, which identified several important SOA precursors (Claeys et al., 2004; Kroll et al., 2006; Lin et al., 2013; Liu, D'Ambro, et al., 2016; Paulot et al., 2009; Ren et al., 2021; Wennberg et al., 2018). The first-generation gas-phase products of isoprene oxidation mainly include hydroxyhydroperoxides (ISOPOOH), methacrolein (MACR), and methyl vinyl ketone (MVK) (Fuchs et al., 2014; Liu et al., 2016; Paulot et al., 2009; Wennberg et al., 2018). Under low NO_x concentrations ([NO_x]), the ratio of the ISOPOOH concentration to the MVK + MACR concentration ([ISOPOOH]/[MVK + MACR]) is in the range of 0.4–0.6 (Liu et al., 2016) Epoxydiols of isoprene (IEPOX) and methacryloylperoxynitrate (MPAN) are the key second-generation intermediates and are formed during isoprene oxidation under low and high [NO_x] conditions, respectively (Lin et al., 2012; Riva et al., 2016b; Surratt et al., 2010). Methacrylic acid epoxide (MAE) and hydroxymethyl-methyl-alpha-lactone (HMML) are also the potential SOA precursors and are derived from the decomposition of MPAN and OH addition products (Lin et al., 2013; Nguyen et al., 2015). The effects of the NO_x concentration on the SOA formation were found to be complicated (Galloway et al., 2011; Jaoui et al., 2021; Newland et al., 2021). NO_x enhanced the SOA yield under low [NO_x] conditions (Kroll et al., 2006) but suppressed the SOA yield under high [NO_x] conditions (Orlando and Tyndall, 2012).

Previous studies indicated that SO_2 enhanced the SOA formation, evidencing the important impact of the interaction between anthropogenic pollutants and biogenic VOC emissions on regional climate (Edney et al., 2005; Kleindienst et al., 2006; Stangl et al., 2019; Surratt et al., 2006, 2007; Ye et al., 2018). The SO_2-derived acidic particles serve as an inorganic acid nucleus to provide more surfaces for the early growth of nano-particles (Chu et al., 2016; Liu et al., 2017). Jang et al. pointed out that the acid-catalyzed heterogeneous reaction has an important contribution to the SOA formation (Jang et al., 2002). SO_2 participates in the SOA formation in the form of organosulfates (Brueggemann et al., 2021; Surratt et al., 2007; Yao et al., 2019), such as the sulfur-containing secondary ozonides via the reaction of SO_2 with Criegee intermediates (CIs) (Vereecken et al., 2012) and RO_2 (Berndt et al., 2015; Lightfoot et al., 1992). The existence of organosulfates in atmospheric particles has been confirmed by laboratory and field sampling studies (Iinuma et al., 2007; Iinuma et al., 2007b; Surratt et al., 2007; Surratt et al., 2008), indicating that SO_2 and acidic particles can modulate the formation and composition of SOA (Lam et al., 2019; Ren et al., 2021; Riva et al., 2016; Shalamzari et al., 2013; Shalamzari et al., 2014; Spolnik et al., 2018; Szmigielski, 2016; Wach et al., 2020; Yang et al., 2023; Zhang et al., 2012). The highly oxidized and fragmented organosulfates can be generated from the reaction of existing organosulfates with OH (Armstrong et al., 2022; Chen et al., 2020), which processes might also produce a strong oxidant of sulfate radical anion (SO_4^-) (Kwong et al., 2018). The interactions of VOCs with SO_4^- have been investigated to address several organosulfates detected in the atmosphere (Noziere et al., 2010; Rudzinski et al., 2009; Schindelka et al., 2013).

In recent decades, many laboratory and field studies have been performed at high concentrations of reactants to investigate the impact of anthropogenic pollutants on the SOA formation from biogenic VOCs under extreme conditions, which contributed to understand the atmospheric processes nearby the emission origins (see the Supporting Information (SI) for more examples). For instance, the smog chamber study at isoprene concentrations of 1.5 and 5 ppm showed that the reaction of known isoprene oxidation products as well as isoprene itself with hydrogen peroxide on or in acidic particles can result in the formation of 2-methyltetrols (Böge et al., 2006). Kleindienst et al. used the concentrated isoprene (8–12.2 ppm) and NO_x (0.3–0.6 ppm) to estimate the SOA contributions of biogenic and anthropogenic hydrocarbons to ambient organic carbon (OC) concentrations, which aided in the development of air quality models (Kleindienst et al., 2007). In the study of Jaoui et al. the concentration of isoprene and O_3 was up to 20.0 and 1.0 ppm, respectively, by which methyl tartaric acid (MTA) was found to serve as a reliable tracer for isoprene (Jaoui et al., 2021).

Pioneering studies on the effects of anthropogenic pollutants on the isoprene photooxidation provided important information for establishing predictive SOA formation networks and improving atmospheric chemical transport models (CTMs) (Kleindienst et al., 2006; Wennberg et al., 2018). Although the enhancement/suppression of NO_x and the enhancement of SO_2 on the SOA formation have been proposed, the combined effect of NO_x and SO_2 on the isoprene photooxidation has not been fully understood yet. Considering that NO is one of the main sinks in RO_2 chemistry (Orlando and Tyndall, 2012), NO was selected as the dominant composition of NO_x in this study. Here, we investigated the individual and combined effects of NO and SO_2 on the SOA formation from the isoprene photooxidation. Combining online vacuum ultraviolet free electron laser (VUV-FEL) photoionization mass spectrometry and quantum chemical calculations, the structures and formation mechanisms of the observed products were analyzed, and the homogeneous

and heterogeneous reaction mechanisms of isoprene photooxidation were discussed. Our results provide important information for fundamental understanding of the initial steps of isoprene oxidation and have important implications for the assessment of photooxidation-induced SOA formation in a complex area with rich vegetation and anthropogenic pollution.

2. Experimental and theoretical methods

Experiments were conducted in the atmosphere simulation DICP-CAS chamber (Dalian Institute of Chemical Physics, Chinese Academy Sciences) with a volume of 2 m^3, which was reported previously (Zang et al., 2022). The experimental methods were detailed in the SI and a brief description was given below. Before all experiments, the chamber was prepared by flushing for 12 h with clean air. The temperature in the chamber was around 296 K, and relative humidity was less than 5%. All the present experiments were performed without the addition of seed aerosols. The liquid isoprene (Aladdin, 99%) was introduced to the smog chamber by injecting it into the airline. After all components were well mixed, the blacklights were turned on, which initiated the photooxidation recorded as the zero time of the experiment.

The concentrations of NO, NO_2, and NO_x were measured by a gas analyzer (Model 42i, Thermo Fisher Scientific, UK), those of SO_2 by a gas analyzer (Model 43i, Thermo Fisher Scientific, UK), and those of O_3 by a gas analyzer (Model 49i, Thermo Fisher Scientific, UK), respectively. The concentrations of isoprene were characterized by proton-transfer reaction mass spectrometer (PTR-QMS 3500, East & West Analytical Instruments, China). The number concentrations and size distributions of particles were measured by a scanning mobility particle sizer spectrometer (SMPS 3938NL76, TSI Incorporated, USA). The aerosol mass losses on smog chamber walls were corrected as described previously (Pathak et al., 2007).

The chemical compositions of the particles were detected by a home-built aerosol time-of-flight mass spectrometer (TOF-MS) based on VUV-FEL photoionization (Zang et al., 2022). A silicone tubing (inner diameter size: 6.35 mm; length: 1 m) was used to connect the reaction chamber and the TOF-MS chamber coupled to the VUV-FEL beamline. The full aerosol population was continuously transported from the reaction chamber to the TOF-MS chamber through aerodynamic lens assembly without pre-separation. Mass spectra of neutral compounds were then measured by threshold photoionization (positive ion mode) with a tunable VUV-FEL.

Geometric optimization and frequency calculations of the intermediates, transition states (TS), and products involved in the reaction pathways were performed using the Gaussian 09 program package (Frisch et al., 2009) at the ωB97XD/aug-cc-pVTZ level of theory (see the SI for theoretical details). The solvation effect was not considered in the present gas-phase calculations.

3. Results and discussion

In the photooxidation experiments of isoprene, the conversion between NO and NO_2 and the effect of $[isoprene]_0/[NO_x]_0$ ratio on the SOA formation were studied by tuning the concentrations of isoprene and NO, respectively. The individual and combined effects of NO and SO_2 on the SOA formation were explored by varying the components of the anthropogenic pollutants. The plausible structures and formation pathways of the products were then analyzed on the basis of VUV-FEL photoionization mass spectra and quantum chemical calculations. The experimental conditions are listed in Table 1. A schematic diagram of reaction pathways is given in Scheme S1 in the SI. The wall loss rate for $[isoprene]_0 = 2.2$, 5.6, 11.0, and 22.0 ppm was 2.3×10^{-5}, 2.8×10^{-5}, 2.8×10^{-5}, and 2.1×10^{-5} s^{-1} (Fig. S1), respectively.

3.1. Effects of NO and SO_2 on particle number concentration and mass concentration

The particle size distributions as a function of the initial concentration of isoprene ($[isoprene]_0$) are shown in Fig. 1. Temporal evolution of the concentration of isoprene and inorganic gases (SO_2, NO_x, and O_3) is illustrated in Figs. S2 and S3, respectively. With the increase of $[isoprene]_0$ from 1.1 ppm to 11 ppm, the moment of particle generation gradually becomes earlier and the time for complete conversion of NO to NO_2 is also shortened. Since the NO conversion by isoprene-derived RO_2 is in competition with the reaction between NO and O_3, the balance of the NO–NO_2–O_3 photolysis cycle is broken, which eventually leads to the accumulation of O_3 (Atkinson, 2000). Namely, the increase of $[isoprene]_0$ accelerates the conversion rate of NO and brings forward the time of the O_3 accumulation. Accordingly, the time for reaching a maximum O_3 concentration ($[O_3]_{max}$) is shorter as marked by the red arrow in Fig. 1.

It can be seen from Fig. 1b-e that the number of nucleation events decreases with the increase of $[isoprene]_0$. Possible reasons are proposed here. Under the condition of 1.1 ppm isoprene (Fig. 1a), isoprene makes little contribution to the O_3 accumulation (Fig. S3). However, the generation of particles was observed at earlier stage of photooxidation as shown in Fig. 1a. Similar finding was also observed at higher concentration of 5.6 ppm isoprene (Fig. S3). These results suggest that the particles generated at this time are dominated by the photooxidation product of SO_2. It is known that SO_2 can be photooxidized to form H_2SO_4, which can participate in the particle formation (Kerminen et al., 2010; Kulmala et al., 2013; Weber et al., 1996). Then, the SOA formation at the early stage might be dominated by acidic particles that are generated from SO_2 oxidation. Upon increasing $[isoprene]_0$ to 1.6 ppm and 2.2 ppm (Fig. 1b and c), the concentration of RO_2 produced by isoprene slightly increases, which enhances the NO_x photolysis cycle. O_3 can be accumulated in a shorter time but be consumed quickly, resulting in the appearance of multiple nucleation events. Under the conditions of 5.6 ppm and 11.0 ppm isoprene (Fig. 1d and e), the number of

Table 1
Overview of the experimental conditions.

$[Isoprene]_0$ (ppm)	$[NO_x]_0$ (ppm)	$[NO]_0$ (ppm)	$[SO_2]_0$ (ppm)	$[Isoprene]_0/[NO_x]_0$	$[O_3]_{max}$ (ppm)	ΔM (μg/m^3)
1.1	0.5	0.5	0.4	2.1	0	25
1.6	0.5	0.5	0.4	3.2	0.1	57
2.2	0.5	0.5	0.4	4.1	0.5	361
5.6	0.5	0.5	0.4	10.5	0.4	544
11.0	0.5	0.5	0.5	21.5	0.2	1159
5.6	0.1	0.1	0.4	54.6	0.1	479
5.6	0.3	0.2	0.4	22.4	0.2	657
5.6	1.1	1.0	0.4	5.1	0.7	2340
5.6	2.1	2.0	0.4	2.6	1.0	926
22.0	1.9	1.7	0.5	11.9	0.3	2653
5.6	0.5	0.5	–	10.5	0.3	155
5.6	–	–	0.4	–	–	128

$[X]_0$: the initial concentration of the species X; $[O_3]_{max}$: the maximum mass concentration of O_3; ΔM: the mass concentration of formed SOA.

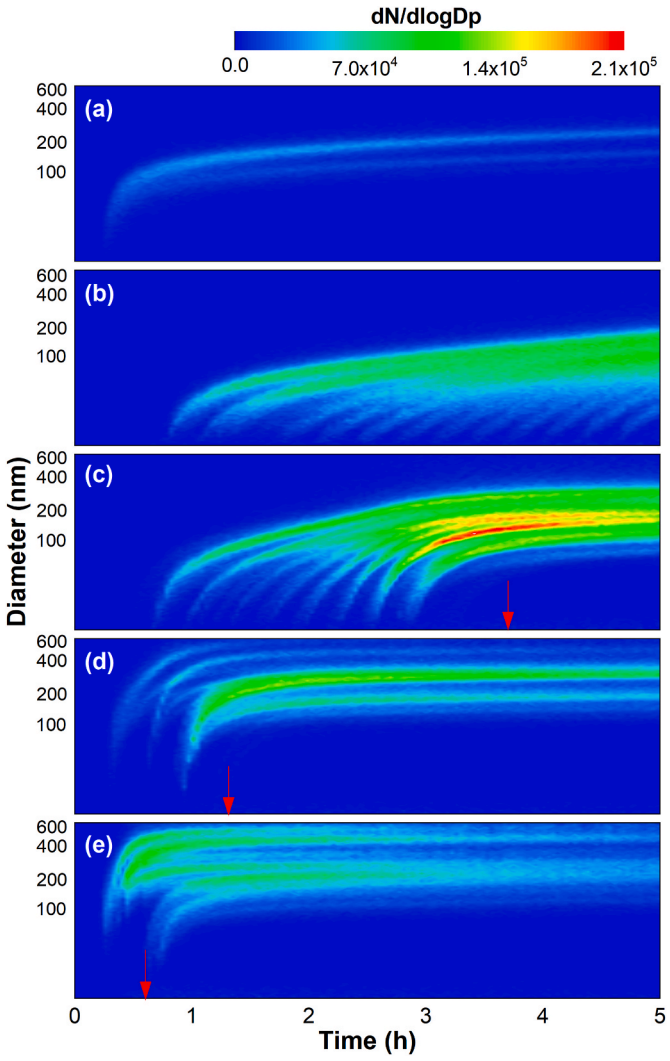

Fig. 1. Temporal evolution of the particle size distribution in the photooxidation experiment based on $[isoprene]_0$ as the main variable at experimental conditions of (a) 1.1 ppm isoprene, 0.5 ppm NO, and 0.4 ppm SO_2; (b) 1.6 ppm isoprene, 0.5 ppm NO, and 0.4 ppm SO_2; (c) 2.2 ppm isoprene, 0.5 ppm NO, and 0.4 ppm SO_2; (d) 5.6 ppm isoprene, 0.5 ppm NO, and 0.4 ppm SO_2; and (e) 11.0 ppm isoprene, 0.5 ppm NO, and 0.5 ppm SO_2. D_p: particle diameter; $dN/dlogD_p$: normalized number size distribution. The moment marked by the red arrow is the time when the $[O_3]$ reaches $[O_3]_{max}$ ((a) no accumulation of O_3 was observed throughout the process; (b) $[O_3]_{max}$ was observed at 5.5 h from the start of the reaction).

nucleation events gradually decrease due to a faster O_3 accumulation rate and higher isoprene concentration, whereas the growth in these two experiments is faster at the beginning than in all other experiments. In these nucleation events, the start of particle generation is synchronized with the beginning of slow consumption of SO_2, suggesting the existence of the particle-phase growth pathway activated by SO_2. The acidic particles also serve as seed aerosols, which likely alter particle production with significant SO_2-isoprene photooxidation. The consumption rate of SO_2 is the fastest during the time period when the accumulation of O_3 starts to reach a maximum value. This indicates that a large number of stabilized Criegee intermediates (sCIs) and RO_2 are produced from the reactions of isoprene with O_3 during the SOA formation, which accelerate the consumption of SO_2 (Kim et al., 2015). The consumption of SO_2 in Fig. 1b-e is 0.1, 0.2, 0.3, and 0.4 ppm, respectively. These findings are consistent with the statement that the SO_2 oxidation by sCIs is an important source of H_2SO_4 in the atmosphere (Boy et al., 2013). In the photooxidation reactions of isoprene with NO and SO_2, NO_x mainly plays two distinct roles. On the one hand, the photolysis of NO_x produces oxidants (i.e., O_3 and OH), which convert gas-phase isoprene and reaction intermediates into particle-phase products, contributing to particle formation. On the other hand, NO serves as the primary sink of RO_2 and consumes RO_2 to form highly volatile organic nitrates, thereby inhibiting the conversion of RO_2 into low-volatility products.

With the increase of $[isoprene]_0$, the particle diameter gradually increases and the rate of particle growth becomes remarkably faster, which are consistent with previous studies (Kroll et al., 2006; Surratt et al., 2006). This could be rationalized that a higher concentration of isoprene leads to a greater number of RO_2 radicals that cause NO to be suppressed more quickly, allowing for $RO_2 + RO_2$ or $RO_2 + HO_2$ termination reactions to dominate and thus nucleating SOA (Kroll et al., 2006; Surratt et al., 2006). Meanwhile, partial products are reactively absorbed by existing particles before they participate in the multi-step oxidation reactions, or the new nuclei condense with each other, resulting in a faster growth of particles. This also explains why the particle number concentration tends to decrease as $[isoprene]_0$ increases from 2.2 ppm to 11.0 ppm.

Fig. 2 shows the O_3 concentration and particle mass concentration as a function of $[isoprene]_0$. It can be seen that the accumulation of O_3 and the change of particle mass concentration are nearly synchronized in time. Note that O_3 is the important product of the atmospheric chemical oxidation processes of VOCs, and its accumulation reflects the pollution status. The O_3 accumulation increases with the increase of $[isoprene]_0$ from 1.1 to 2.2 ppm and then decreases with $[isoprene]_0$ up to 11.0 ppm. These observations show that more O_3 would be probably accumulated by long-term photooxidation reactions in the environments with serious NO_x and SO_2 pollution and rich vegetation, which enhances the oxidation capacity of the troposphere in the corresponding area and thereby aggravates the air pollution. The increase trend of particle mass concentration with increasing $[isoprene]_0$ indicates that the degree of oxidation reaction is enhanced at higher isoprene concentration. The particle size distributions as a function of $[NO]_0$ are shown in Fig. S4. With the increase of $[NO]_0$, the conversion time of NO gradually becomes longer. The particle number concentration reaches at a maximum value when $[NO]_0$ is 0.1 ppm.

The maximum concentration of O_3 and the mass concentration of formed SOA (ΔM) as a function of the $[isoprene]_0/[NO_x]_0$ ratio are shown in Fig. 3. With the increase of $[isoprene]_0$ (Fig. 3a), $[O_3]_{max}$ increases with increasing the $[isoprene]_0/[NO_x]_0$ ratio, reaches a maximum value at $[isoprene]_0/[NO_x]_0 = 4.1$, and then decreases with

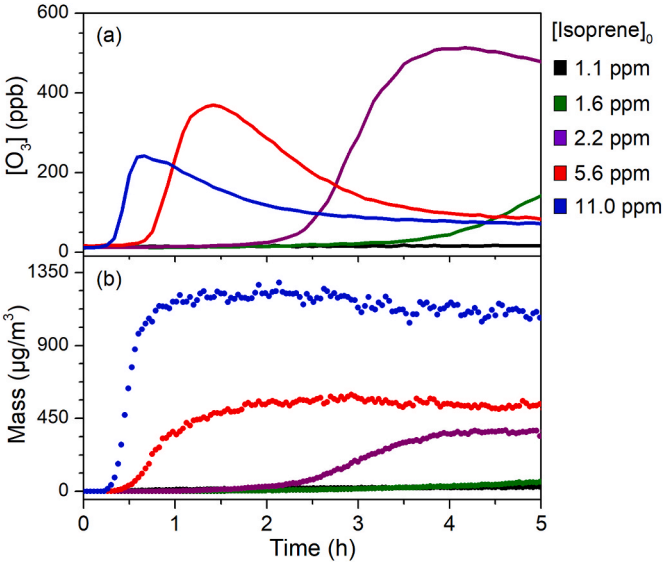

Fig. 2. The O_3 concentration and particle mass concentration as a function of $[isoprene]_0$.

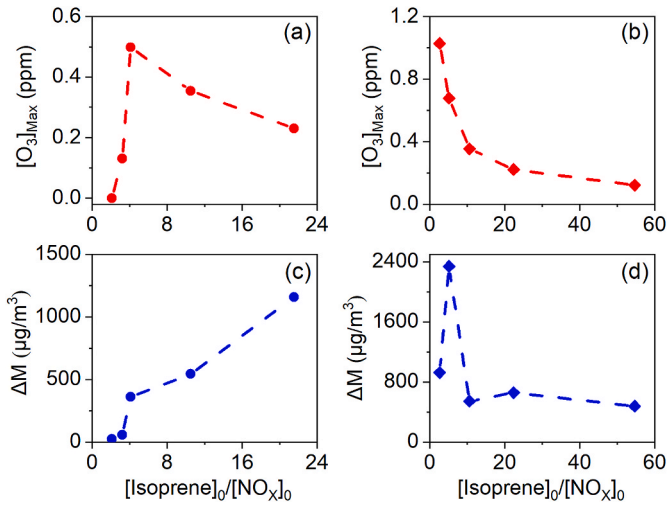

Fig. 3. $[O_3]_{max}$ (a and b) and mass concentration of formed SOA (ΔM) (c and d) as a function of $[isoprene]_0/[NO_x]_0$. The dot and square icons represent the change of $[isoprene]_0$ and $[NO]_0$, respectively.

further increasing the $[isoprene]_0/[NO_x]_0$ ratio. The increase of $[O_3]_{max}$ indicates that the formation of O_3 is faster than the consumption of O_3 at $[isoprene]_0/[NO_x]_0 < 4.1$ ($[isoprene]_0$: 1.1–2.2 ppm). With further increase of $[isoprene]_0$, even though the conversion of NO is accelerated, the higher initial concentration of isoprene leads to more consumption of O_3, resulting in a decrease trend of $[O_3]_{max}$. Thus, the accumulation of O_3 becomes difficult, and the mass concentration gradually increases (Fig. 3c). As illustrated in Fig. 3b and d, with the decrease of $[NO]_0$, the amount of O_3 accumulated by NO_2 photolysis becomes smaller, and the mass concentration changes in a parabolic trend. This indicates that under low NO_x condition, increasing $[NO]_0$ in a small range produces higher $[O_3]$ through photolysis of NO_2, which promotes the oxidation reaction of isoprene and thereby enhances the mass concentration of SOA. Continuing to increase $[NO]_0$, although the cumulative O_3 concentration increases, the inhibition effect of NO_x on the oxidation of isoprene is more pronounced, leading to a decrease in mass concentration.

The individual and combined effects of NO and SO_2 on the particle size distributions are compared in Fig. S5 and the $[SO_2]$, $[NO_x]$, and $[O_3]$ as a function of time are shown in Fig. S6. In the photooxidation reaction of isoprene and SO_2 (Fig. S5a), the particulate matter is mainly dominated by acidic particles formed by SO_2 photooxidation, and the start time of the nucleation events is 0.3 h. In the photooxidation reaction with isoprene and NO (Fig. S5b), the start time of the nucleation event is postponed to 1.3 h. In the photooxidation of isoprene in the presence of both NO and SO_2 (Fig. S5c), the photooxidation is significantly different compared to that in the absence of SO_2. The nucleation events started at 0.3 h, and occurred three times. At 3 h, the largest size of particles formed with SO_2 is about 600 nm (Fig. S5c), which is much larger than that of particles formed without SO_2 (Fig. S5b, about 360 nm). Furthermore, we conducted a series of comparative experiments without SO_2. The experimental conditions are listed in Table S1. The temporal evolution of the particle size distributions in the isoprene and NO photooxidation reactions without SO_2 are shown in Fig. S7 (as a function of $[isoprene]_0$) and S8 (as a function of $[NO]_0$). In the experiments without SO_2, only one nucleation event was observed (Figs. S7c, S7d, and S7e) and the particle size was smaller as compared to the experiments with SO_2 (Fig. 1). Under the conditions of 1.1/1.6 ppm + 0.5 ppm NO (Figs. S7a and S7b), no particles were observed, whereas lots of particles were observed in the experiments with SO_2 (Fig. 1a and b). In addition, the mass concentration of particles produced in the experiments without SO_2 (Table S1) is obviously lower than that of particle produced in the experiments with SO_2 (Table 1). These results indicate that the presence of SO_2 promotes the nucleation and growth of particle. As listed in Table S1, $t_{[O3]max}$ is remarkably shortened in the experiments with SO_2, indicating that the presence of SO_2 can significantly accelerate the conversion of NO. In the previous studies (Lin et al., 2012; Surratt et al., 2010), IEPOX is the key precursor derived from the photooxidation of isoprene in the presence of acidified sulfate seed aerosol. In the present study, SO_2 was quickly oxidized to form acidic particles after triggering the photooxidation reaction. However, no product peaks in the particle phase were detected until NO was fully transformed. This does not necessarily imply that related products were not produced, or the instrument may not respond efficiently because the product concentration is too low. After the NO conversion, distinct peaks in the aerosol mass spectra were observed, which could be attributed to the high concentration of particle-phase product during this period. However, it should be noted that the primary reaction during this time is the oxidation of isoprene and O_3. Nevertheless, the acid-driven multiphase chemistry of IEPOX and the formation of other isoprene-derived oxidation products cannot be ruled out.

3.2. *VUV-FEL photoionization mass spectra of isoprene photooxidation*

The compounds generated from the isoprene photooxidation were measured by VUV-FEL photoionization aerosol mass spectrometer. Considering that the VUV-FEL beamline time is very expensive and the reaction time of isoprene with NO and SO_2 is shorter at high concentrations than that at low concentrations, the VUV-FEL photoionization mass spectra of the compounds were thus measured at higher concentrations of isoprene, NO, and SO_2 than atmospheric conditions. Various experimental conditions (the wavelength and pulse energy of VUV-FEL, the concentrations of isoprene, NO, and SO_2, etc.) were optimized to find an optimum experimental conditions. The VUV-FEL pulse energy dependence was measured to avoid the saturation of photoionization. The fragmentation and reactions caused in the VUV-FEL photoionization are negligible, which have been confirmed by our previous mass spectrometric studies of aerosols (Zang et al., 2022) and infrared spectroscopic study of neutral clusters (Jiang et al., 2021; Wang et al., 2022, 2023; Zhang et al., 2020). The detection limit of aerosol is about 0.3 mmol/L.

Fig. S9 shows the 100.0, 104.0, and 108.0 nm mass spectra of the compounds generated at the condition of 1.1 ppm isoprene, 0.5 ppm NO, and 0.4 ppm SO_2. The mass peaks with higher intensities are observed at 100.0 nm (Fig. S9a). When tuning the VUV-FEL wavelength to 104.0 nm, most of the signals disappear (Fig. S9b). No obvious peaks are observed at 108.0 nm (Fig. S9c). These results demonstrate that the tunable VUV-FEL (50–150 nm, 8.3–24.8 eV) allows for selective photoionization of neutral compounds with different ionization energies, which may uncover SOA components that were not detected by conventional ionization methods in previous studies.

Fig. 4 shows the 100.0 nm photoionization mass spectra of the compounds under conditions of continuous increase in the concentration of isoprene, NO_x, and SO_2. The positions and intensities of these mass peaks are listed in Table S2. As shown in Fig. 4a, the intensities of mass spectral peaks at the condition (a) are weak, which is consistent with no obvious O_3 accumulation within 8 h at low $[isoprene]_0$ as aforementioned and supports the inference that lower $[O_3]$ leads to lower mass concentration of particles. In contrast with the mass spectra at the condition (b) (Fig. 4b), the intensities of mass spectral peaks at the condition (c) (Fig. 4c) are higher for the $m/z < 130$ compounds.

O_3 produced by NO favorably triggers the isoprene ozonolysis, and derives the secondary oxidant OH. O_3 and OH are beneficial to the transformation of isoprene into particle phase products. The isoprene with higher concentration produces more RO_2 and thus consumes more NO, which affects the production source of the oxidants (O_3 and OH). In this complex photooxidation cycle, the effects of NO and isoprene compete with each other and affect the SOA formation. For Fig. 4c and b, the simultaneous increase of isoprene and NO concentrations has a more

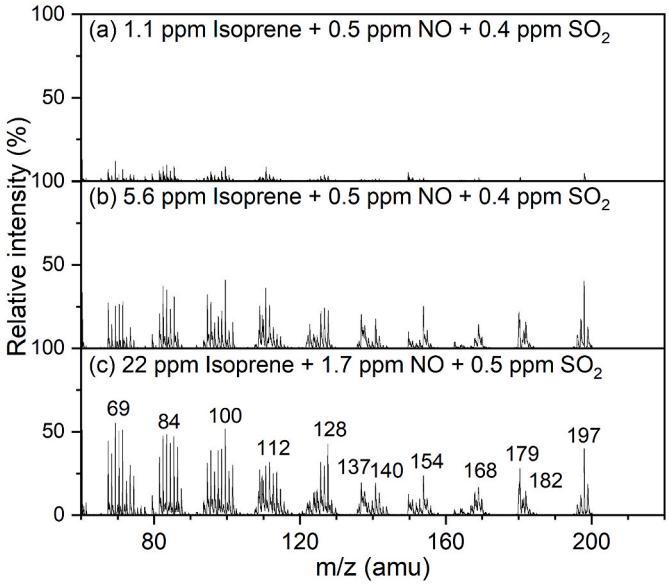

Fig. 4. VUV-FEL photoionization mass spectra of the compounds generated under different experimental conditions. The compounds were ionized by the VUV-FEL at 100.0 nm.

obvious inhibitory effect on SOA formation. This suggests that the entire photooxidation process is suppressed due to the excessively high [NO], even though the $[isoprene]_0$ is increased. The mass concentration and number concentration of particles also decay significantly after reaching $[O_3]_{max}$, which may be attributed to the cleavage of smaller alkoxy groups (RO) and the relative volatility of organic nitrates. The higher intensities of the $m/z < 130$ peaks are due to the higher initial reactant concentrations and faster response, resulting in the rapid growth of mass concentration. This promotes the absorption or condensation of a large number of less oxidized products on the surface of existing particles, which can be detected by the VUV-FEL photoionization. As listed in Table S2, the intensities of the peaks at m/z = 137, 154, 182, and 197 in Fig. 4c are slightly smaller than those in Fig. 4b. It can be seen from Fig. 4 that there is no significant change of peak positions among these three mass spectra, indicating that the initial concentrations of isoprene and NO have little effects on chemical compositions of the compounds.

3.3. Composition analysis of the compounds formed from isoprene photooxidation

In order to elucidate the main pathways of the photooxidation products of isoprene, the individual effects of NO and SO_2 on the SOA formation were investigated by VUV-FEL photoionization mass spectrometry and the results are shown in Fig. 5. The peak intensities are relatively higher for isoprene photooxidation in the presence of both NO and SO_2 (Fig. 5c) and decrease significantly by about 6 times for isoprene photooxidation by only NO_x (Fig. 5b), indicating the importance of SO_2 in the processes of atmospheric photooxidation. As pointed out previously (Kleindienst et al., 2006), gas-phase isoprene are largely unaffected by SO_2 when it reacts only with SO_2. The slow consumption of isoprene is attributed to wall loss and condensation on the acidic seed aerosol generated by SO_2. Indeed, no obvious mass peaks are observed for isoprene photooxidation by only SO_2 as shown in Fig. 5a.

To analyze the possible sources of the observed compounds, the structures and formation pathways of the $m/z > 120$ compounds are proposed with the aid of quantum chemical calculations. The $m/z = 134$, 137, 150, 152, and 179 compounds are newly-observed species, which are marked in red in Fig. 5. The possible formation mechanisms of these new species are shown in Fig. 6, which pathways are not exclusive. While O_3 is the main oxidant in this study as mentioned above, MACR

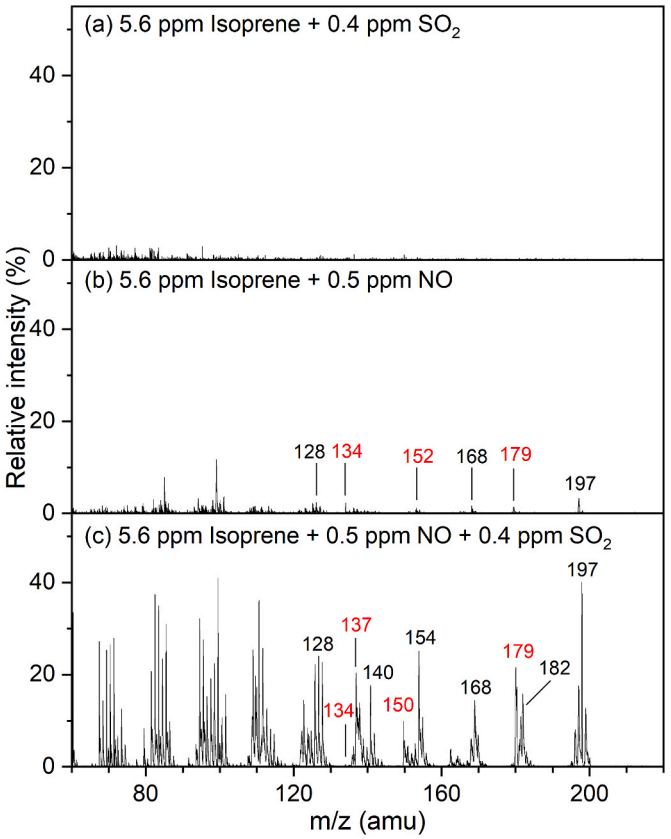

Fig. 5. VUV-FEL photoionization mass spectra of the compounds generated under different experimental conditions. The compounds were ionized by the VUV-FEL 100.0 nm.

($m/z = 70$) is one of the main ozonolysis products of isoprene as identified in previous PTR mass spectra (Lin et al., 2012). Zhang et al. proposed that OH can be obtained by rapid thermal decomposition of carbonyl oxides in the reaction between isoprene and O_3, and the estimated yield can reach 0.25 (Zhang and Zhang, 2002). As the main oxidant generated by the secondary reaction in these experiments, the OH radical immediately initiates the oxidation reaction with isoprene.

The carbon center radical generated from the reaction between MACR and OH reacts with O_2 to form RO_2, and further reacts with HO_2 to produce the intermediate **1**, which process is calculated to be highly exothermic by 87.6 kcal/mol. The intermediate **2** is generated by the H-abstraction from **1** with an exothermic value of 111.4 kcal/mol, and is subsequently oxidized to form **3** with an exothermic value of 54.3 kcal/mol. RO_2 undergoes bimolecular reaction with NO and HO_2 to form products **P1** ($m/z = 179$) and **P2** ($m/z = 150$), releasing energy of 53.9 and 46.6 kcal/mol, respectively. With the change of experimental condition from Fig. 5c to b, the mass spectral intensities of **P1** and **P2** are remarkably reduced. It shows that with the removal of SO_2, more amount of HO_2 might be consumed in the conversion process of NO ($HO_2 + NO \rightarrow OH + NO_2$), which reduces the **3** + NO → **P1** and **3** + HO_2 → **P2** reactions. Since **P3** ($m/z = 152$) is weakly observed in the isoprene photooxidation under the presence of NO (Fig. 5b), its possible formation mechanism could be that **4** is formed by the oxidation of **1** with an exothermic value of 57.5 kcal/mol, and then reacts with HO_2 to form **P3** with an exothermic value of 45.3 kcal/mol. Note that the conversion time of NO to NO_2 with and without the presence of SO_2 is about 1.3 and 1.5 h (Fig. S6), respectively, which indicates that SO_2 can promote the conversion of NO. As pointed out above, **P3** is observed just after the complete conversion of NO, indicating that the **4** + HO_2 reaction is more favorable to proceed after the long-term conversion of NO is finished. In comparison, **P1**, as the termination product of the RO_2 + NO reaction, is

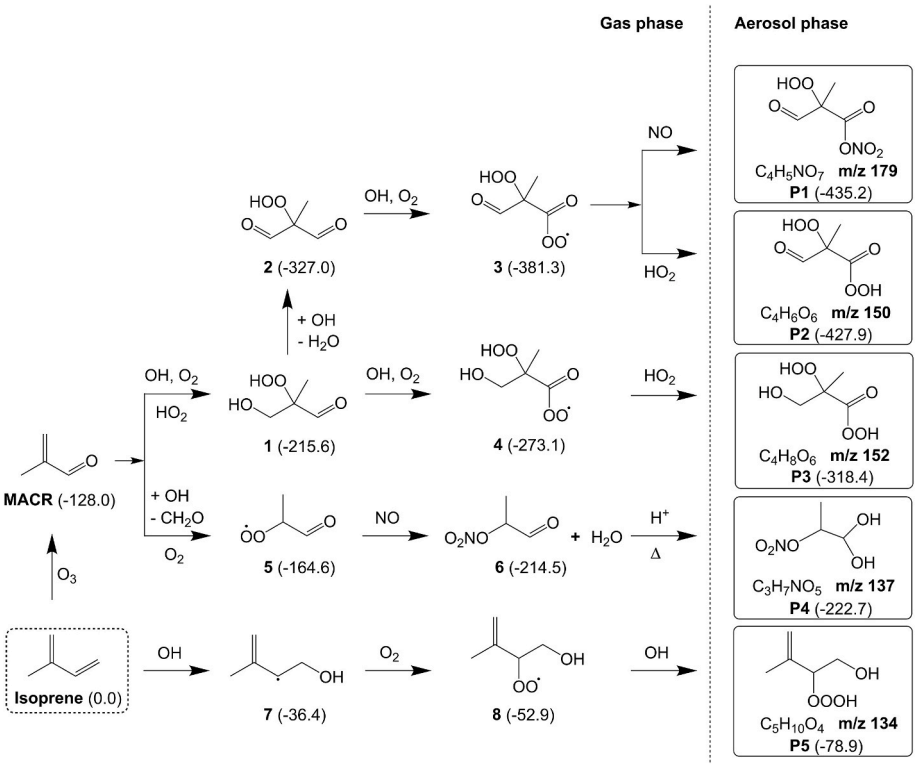

Fig. 6. Possible formation mechanism of newly-observed species calculated at the ωB97XD/aug-cc-pVTZ level of theory. Relative energies are given in kcal/mol.

readily formed owing to the advantages of its lower relative energy.

It can be seen from Fig. 5c that there is a relatively high proportion of **P4** (m/z = 137) in the presence of SO_2, which formation path could be affected by SO_2. MACR undergoes an addition reaction with OH, and then releases CH_2O with an energy barrier of 11.8 kcal/mol, resulting in the formation of the intermediate **5** through autoxidation. This overall process is predicted to be exothermic by 36.6 kcal/mol **5** reacts with NO to produce **6**, which is exothermic by 49.9 kcal/mol **6** contains an aldehyde group, which undergoes the hydration reaction to form **P4** by proton transfer under acid-catalyzed conditions (Fig. S10), which is exothermic by 8.2 kcal/mol with a small barrier of 7.5 kcal/mol. As one of the unique product peaks in the presence of SO_2, **P4** (m/z = 137) might be generated from the heterogeneous reaction on the surface of the acidic particles.

The relative intensity of **P5** (m/z = 134) in Fig. 5c is remarkably smaller than that in Fig. 5b, indicating that the formation of **P5** would be suppressed by SO_2. In the process of online mass spectrometry detection, **P5** is observed before the end of NO conversion; when O_3 begins to accumulate, the intensity of **P5** gradually decrease whereas those of m/z = 168, 179, 197 and other products increase. This suggests that **P5** may be originated from the oxidation of isoprene at low concentration of OH during the long-term conversion of NO. If the concentration of SO_2 is high, on the one hand, it consumes OH to compete with the formation path of **P5**; on the other hand, it accelerates the conversion of NO and promotes the accumulation of O_3 to reduce the formation of **P5**. As shown in Fig. 6, isoprene undergoes an addition reaction with OH to produce **7**, which further autoxidizes to form **8** with an exothermic value of 52.9 kcal/mol. Then, **8** reacts with OH to form **P5** with an OOOH group, which process is exothermic by 23.0 kcal/mol. The reaction of RO_2 with OH has the rate coefficient close to the collision limit, and the atmospheric lifetime of hydrotrioxide (ROOOH) was estimated to be in the range of minutes to hours (Berndt et al., 2022).

On the basis of the structures of the m/z = 197, 182, 168, 154, 140, and 128 compounds proposed in previous studies (Amaladhasan et al., 2022; Fang et al., 2012; Liu, D'Ambro, et al., 2016; Spolnik et al., 2018; Wach et al., 2020), their plausible formation pathways are shown in Figs. S11 and S12, respectively. Previous studies have suggested that **P6** (m/z = 197) and **P7** (m/z = 168) are the oxidation products of isoprene and OH under the presence of NO, and the abundance of **P6** and **P7** is affected by [NO] (Liu, D'Ambro, et al., 2016). In the present experiments, these two compounds are observed at the end of NO conversion, and the relative intensity of **P7** increases after $[O_3]$ reaches $[O_3]_{max}$, which does not rule out that there are products with the same mass produced by oxidation through the ozone pathway, such as the 2-hydroxy-dihydroperoxide ($C_5H_{12}O_6$) proposed in previous studies (Amaladhasan et al., 2022). We analyzed the possible formation path of **P8** (m/z = 128) based on the structures proposed by Sheng et al. (Fang et al., 2012) **P9** (**P9'**) (m/z = 182), **P10** (m/z = 154), and **P11** (m/z = 140) are unique peaks in the presence of SO_2 and probably formed from the oxidation reaction of isoprene and SO_4^-. **14** (**14′**) are stemmed from the addition of isoprene and SO_4^-. **P9** (**P9'**) containing unsaturated double bonds is generated by further autoxidation and H-addition of **14** (**14′**), which is calculated to be extremely exothermic by 126.7 kcal/mol (129.0 kcal/mol). **P9** (**P9'**) proceeds multi-step reactions with SO_4^-, O_2, and NO, cyclization reaction with the release of H_2SO_3 to generate **17** (**17′**) ($C_5H_{10}O_7S$, m/z = 214), and cleavage reaction to form **P10** and **P11**. The products **P9** (**P9'**), **17** (**17′**), and the fragments **P10** and **P11** have been identified as evidentiary organosulfates derived from isoprene in previous studies (Spolnik et al., 2018; Wach et al., 2020). It should be noted that a large amount of RO_2 are also derived from the reaction between isoprene and SO_4^-, which convert NO into NO_2. As mentioned above, the presence of SO_2 shortens the conversion time of NO in the photooxidation process by about 0.2 h.

4. Conclusions and atmospheric implications

In this study, the effects of NO and SO_2 on the mass concentrations, particle number concentrations, and chemical compositions of SOA formation were explored by a number of laboratory studies for isoprene photooxidation. It is found that the accumulated O_3 originated from the

NO conversion triggers the main oxidation reaction, by which the oxidants (i.e., OH and SO_4^-) are derived. In the absence of SO_2, the **P1**, **P3**, and **P7** ($m/z = 179, 152, 168$) compounds are formed through the cross-oxidation channels of isoprene with O_3 and OH; **P5**, **P6**, **P7**, and **P8** ($m/z = 134, 197, 168, 128$) are produced via the oxidation reaction of isoprene with OH. These products further oligomerize to form species with lower volatility or/and undergo a homogeneous nucleation process, eventually forming SOA in the absence of seed aerosols. In the presence of SO_2, **P1**, **P2**, **P6**, and **P7** ($m/z = 179, 150, 152, 197, 168$) are formed through cross-oxidation channels of isoprene with O_3 and OH; **P9**, **P10**, and **P11** ($m/z = 182, 154, 140$) are generated from the reaction of isoprene with SO_4^-; **P4** ($m/z = 137$) is formed by a heterogeneous reaction. The homogeneous reaction processes under this condition include: mutual polymerization and nucleation of low-volatility products formed by isoprene oxidation; SO_2 is oxidized by OH and sCIs to produce H_2SO_4 in the gas phase, and finally condenses with other substances to form acidic particles; organicsulfates are formed by the reaction of intermediates with derivatives of SO_2 (H_2SO_4 or SO_4^-). Heterogeneous reaction processes include the catalytic reaction by employing H_2SO_4 on the surface of acidic particles and the adsorption or absorption of gas and semi-volatile products on the surface of particles. The present results support the insights proposed in previous studies, and also demonstrate the importance of the synergistic effects of NO and SO_2 in the atmosphere, which help to advance mechanical understanding of atmospheric components affected by the anthropogenic-biogenic interactions nearby the emission origins, especially under extreme conditions.

CRediT authorship contribution statement

Zhaoyan Zhang: Data curation, Formal analysis, Investigation, Methodology, Writing – original draft, Conceptualization. **Yingqi Zhao:** Data curation, Formal analysis, Investigation, Software. **Ya Zhao:** Data curation, Investigation, Visualization. **Xiangyu Zang:** Data curation, Formal analysis, Investigation. **Hua Xie:** Formal analysis, Funding acquisition, Validation. **Jiayue Yang:** Resources, Validation. **Weiqing Zhang:** Resources, Validation. **Guorong Wu:** Resources, Validation. **Gang Li:** Conceptualization, Funding acquisition, Investigation, Project administration, Supervision, Validation, Visualization, Writing – original draft, Writing – review & editing. **Xueming Yang:** Funding acquisition, Project administration, Resources, Validation. **Ling Jiang:** Conceptualization, Data curation, Formal analysis, Funding acquisition, Investigation, Methodology, Project administration, Supervision, Validation, Visualization, Writing – original draft, Writing – review & editing.

Declaration of competing interest

The authors declare the following financial interests/personal relationships which may be considered as potential competing interests:

Ling Jiang reports financial support was provided by National Natural Science Foundation of China.

Data availability

Data will be made available on request.

Acknowledgments

The authors gratefully acknowledge the Dalian Coherent Light Source (DCLS) for support and assistance. This work was supported by the National Natural Science Foundation of China (Grant Nos. 92361302, 92061203, 22125303, 22103082, 22273101, 22288201 and 21327901), the National Key Research and Development Program of China (No. 2021YFA1400501), Innovation Program for Quantum Science and Technology (No. 2021ZD0303304), Dalian Institute of Chemical Physics (No. DICP DCLS201702), Chinese Academy of Sciences (No. GJJSTD20220001), International Partnership Program of CAS (121421KYSB20170012), and K. C. Wong Education Foundation (No. GJTD-2018-06).

Appendix A. Supplementary data

Supplementary data to this article can be found online at https://doi.org/10.1016/j.atmosenv.2023.120248.

References

Amaladhasan, D.A., Heyn, C., Hoyle, C.R., El Haddad, I., Elser, M., Pieber, S.M., et al., 2022. Modelling the gas-particle partitioning and water uptake of isoprene-derived secondary organic aerosol at high and low relative humidity. Atmos. Chem. Phys. 22 (1), 215–244.

Arashiro, M., Lin, Y.-H., Sexton, K.G., Zhang, Z., Jaspers, I., Fry, R.C., et al., 2016. In vitro exposure to isoprene-derived secondary organic aerosol by direct deposition and its effects on COX-2 and IL-8 gene expression. Atmos. Chem. Phys. 16 (22), 14079–14090.

Armstrong, N.C., Chen, Y., Cui, T., Zhang, Y., Christensen, C., Zhang, Z., et al., 2022. Isoprene epoxydiol-derived sulfated and nonsulfated oligomers suppress particulate mass loss during oxidative aging of secondary organic aerosol. Environ. Sci. Technol. 56 (23), 16611–16620.

Atkinson, R., 2000. Atmospheric chemistry of VOCs and NO_X. Atmos. Environ. 34 (12–14), 2063–2101.

Atkinson, R., Baulch, D.L., Cox, R.A., Crowley, J.N., Hampson, R.F., Hynes, R.G., et al., 2006. Evaluated kinetic and photochemical data for atmospheric chemistry: volume II - gas phase reactions of organic species. Atmos. Chem. Phys. 6, 3625–4055.

Berndt, T., Richters, S., Kaethner, R., Voigtlaender, J., Stratmann, F., Sipilae, M., et al., 2015. Gas-phase ozonolysis of cycloalkenes: formation of highly oxidized RO_2 radicals and their reactions with NO, NO_2, SO_2, and other RO_2 radicals. J. Phys. Chem. A 119 (41), 10336–10348.

Berndt, T., Chen, J., Kjaergaard, E.R., Moller, K.H., Tilgner, A., Hoffmann, E.H., et al., 2022. Hydrotrioxide (ROOOH) formation in the atmosphere. Science 376 (6596), 979–982.

Böge, O., Miao, Y., Plewka, A., Herrmann, H., 2006. Formation of secondary organic particle phase compounds from isoprene gas-phase oxidation products: an aerosol chamber and field study. Atmos. Environ. 40 (14), 2501–2509.

Boy, M., Mogensen, D., Smolander, S., Zhou, L., Nieminen, T., Paasonen, P., et al., 2013. Oxidation of SO_2 by stabilized Criegee intermediate (sCI) radicals as a crucial source for atmospheric sulfuric acid concentrations. Atmos. Chem. Phys. 13 (7), 3865–3879.

Brauer, M., Freedman, G., Frostad, J., van Donkelaar, A., Martin, R.V., Dentener, F., et al., 2016. Ambient air pollution exposure estimation for the global burden of disease 2013. Environ. Sci. Technol. 50 (1), 79–88.

Brueggemann, M., Riva, M., Perrier, S., Poulain, L., George, C., Herrmann, H., 2021. Overestimation of monoterpene organosulfate abundance in aerosol particles by sampling in the presence of SO_2. Environ. Sci. Technol. Lett. 8 (3), 206–211.

Bryant, D.J., Dixon, W.J., Hopkins, J.R., Dunmore, R.E., Pereira, K., Shaw, M., et al., 2020. Strong anthropogenic control of secondary organic aerosol formation from isoprene in Beijing. Atmos. Chem. Phys. 20 (12), 7531–7552.

Chen, Y., Zhang, Y., Lambe, A.T., Xu, R., Lei, Z., Olson, N.E., et al., 2020. Heterogeneous hydroxyl radical oxidation of isoprene-epoxydiol-derived methyltetrol sulfates: plausible formation mechanisms of previously unexplained organosulfates in ambient fine aerosols. Environ. Sci. Technol. Lett. 7 (7), 460–468.

Chu, B., Zhang, X., Liu, Y., He, H., Sun, Y., Jiang, J., et al., 2016. Synergetic formation of secondary inorganic and organic aerosol: effect of SO_2 and NH_3 on particle formation and growth. Atmos. Chem. Phys. 16 (22), 14219–14230.

Claeys, M., Graham, B., Vas, G., Wang, W., Vermeylen, R., Pashynska, V., et al., 2004. Formation of secondary organic aerosols through photooxidation of isoprene. Science 303 (5661), 1173–1176.

Dommen, J., Metzger, A., Duplissy, J., Kalberer, M., Alfarra, M.R., Gascho, A., et al., 2006. Laboratory observation of oligomers in the aerosol from isoprene/NO_x photooxidation. Geophys. Res. Lett. 33 (13).

Eaves, L.A., Smeester, L., Hartwell, H.J., Lin, Y.-H., Arashiro, M., Zhang, Z., et al., 2020. Isoprene-derived secondary organic aerosol induces the expression of microRNAs associated with inflammatory/oxidative stress response in lung cells. Chem. Res. Toxicol. 33 (2), 381–387.

Edney, E.O., Kleindienst, T.E., Jaoui, M., Lewandowski, M., Offenberg, J.H., Wang, W., et al., 2005. Formation of 2-methyl tetrols and 2-methylglyceric acid in secondary organic aerosol from laboratory irradiated isoprene/NO_X/SO_2/air mixtures and their detection in ambient $PM_{2.5}$ samples collected in the eastern United States. Atmos. Environ. Times 39 (29), 5281–5289.

Ehn, M., Thornton, J.A., Kleist, E., Sipila, M., Junninen, H., Pullinen, I., et al., 2014. A large source of low-volatility secondary organic aerosol. Nature 506 (7489), 476–479.

Fang, W.Z., Gong, L., Zhang, Q., Cao, M.Q., Li, Y., Sheng, L.S., 2012. Measurements of secondary organic aerosol formed from OH-initiated photo-oxidation of isoprene using online photoionization aerosol mass spectrometry. Environ. Sci. Technol. 46 (7), 3898–3904.

Frisch, M.J., Trucks, G.W., Schlegel, H.B., Scuseria, G.E., Robb, M.A., Cheeseman, J.R., et al., 2009. Gaussian 09. Gaussian. CT, Inc., Wallingford.
Fuchs, H., Acir, I.H., Bohn, B., Brauers, T., Dorn, H.P., Haeseler, R., et al., 2014. OH regeneration from methacrolein oxidation investigated in the atmosphere simulation chamber SAPHIR. Atmos. Chem. Phys. 14 (15), 7895–7908.
Galloway, M.M., Huisman, A.J., Yee, L.D., Chan, A.W.H., Loza, C.L., Seinfeld, J.H., et al., 2011. Yields of oxidized volatile organic compounds during the OH radical initiated oxidation of isoprene, methyl vinyl ketone, and methacrolein under high-NO_x conditions. Atmos. Chem. Phys. 11 (21), 10779–10790.
Guenther, A.B., Jiang, X., Heald, C.L., Sakulyanontvittaya, T., Duhl, T., Emmons, L.K., et al., 2012. The model of emissions of gases and aerosols from nature version 2.1 (MEGAN2.1): an extended and updated framework for modeling biogenic emissions. Geosci. Model Dev. (GMD) 5 (6), 1471–1492.
Hallquist, M., Wenger, J.C., Baltensperger, U., Rudich, Y., Simpson, D., Claeys, M., et al., 2009. The formation, properties and impact of secondary organic aerosol: current and emerging issues. Atmos. Chem. Phys. 9 (14), 5155–5236.
Heinritzi, M., Dada, L., Simon, M., Stolzenburg, D., Wagner, A.C., Fischer, L., et al., 2020. Molecular understanding of the suppression of new-particle formation by isoprene. Atmos. Chem. Phys. 20 (20), 11809–11821.
Iinuma, Y., Mueller, C., Boege, O., Gnauk, T., Herrmann, H., 2007a. The formation of organic sulfate esters in the limonene ozonolysis secondary organic aerosol (SOA) under acidic conditions. Atmos. Environ. 41 (27), 5571–5583.
Iinuma, Y., Muller, C., Berndt, T., Boge, O., Claeys, M., Herrmann, H., 2007b. Evidence for the existence of organosulfates from beta-pinene ozonolysis in ambient secondary organic aerosol. Environ. Sci. Technol. 41 (19), 6678–6683.
Jang, M.S., Czoschke, N.M., Lee, S., Kamens, R.M., 2002. Heterogeneous atmospheric aerosol production by acid-catalyzed particle-phase reactions. Science 298 (5594), 814–817.
Jaoui, M., Piletic, I.R., Szmigielski, R., Rudzinski, K.J., Lewandowski, M., Riedel, T.P., et al., 2021. Rapid production of highly oxidized molecules in isoprene aerosol via peroxy and alkoxy radical isomerization pathways in low and high NO_x environments: combined laboratory, computational and field studies. Sci. Total Environ. 775, 145592.
Jiang, S., Su, M., Yang, S., Wang, C., Huang, Q.-R., Li, G., et al., 2021. Vibrational signature of dynamic coupling of a strong hydrogen bond. J. Phys. Chem. Lett. 12 (9), 2259–2265.
Kerminen, V.M., Petaja, T., Manninen, H.E., Paasonen, P., Nieminen, T., Sipila, M., et al., 2010. Atmospheric nucleation: highlights of the EUCAARI project and future directions. Atmos. Chem. Phys. 10 (22), 10829–10848.
Kim, S., Guenther, A., Lefer, B., Flynn, J., Griffin, R., Rutter, A.P., et al., 2015. Potential role of stabilized Criegee radicals in sulfuric acid production in a high biogenic VOC environment. Environ. Sci. Technol. 49 (6), 3383–3391.
Kleindienst, T.E., Edney, E.O., Lewandowski, M., Offenberg, J.H., Jaoui, M., 2006. Secondary organic carbon and aerosol yields from the irradiations of isoprene and alpha-pinene in the presence of NO_x and SO_2. Environ. Sci. Technol. 40 (12), 3807–3812.
Kleindienst, T.E., Jaoui, M., Lewandowski, M., Offenberg, J.H., Lewis, C.W., Bhave, P.V., et al., 2007. Estimates of the contributions of biogenic and anthropogenic hydrocarbons to secondary organic aerosol at a southeastern US location. Atmos. Environ. 41 (37), 8288–8300.
Kramer, A.J., Rattanavaraha, W., Zhang, Z., Gold, A., Surratt, J.D., Lin, Y.-H., 2016. Assessing the oxidative potential of isoprene-derived epoxides and secondary organic aerosol. Atmos. Environ. 130, 211–218.
Kroll, J.H., Ng, N.L., Murphy, S.M., Flagan, R.C., Seinfeld, J.H., 2005. Secondary organic aerosol formation from isoprene photooxidation under high-NO_x conditions. Geophys. Res. Lett. 32 (18), L18808.
Kroll, J.H., Ng, N.L., Murphy, S.M., Flagan, R.C., Seinfeld, J.H., 2006. Secondary organic aerosol formation from isoprene photooxidation. Environ. Sci. Technol. 40 (6), 1869–1877.
Kulmala, M., Kontkanen, J., Junninen, H., Lehtipalo, K., Manninen, H.E., Nieminen, T., et al., 2013. Direct observations of atmospheric aerosol nucleation. Science 339 (6122), 943–946.
Kwok, E.S.C., Aschmann, S.M., Arey, J., Atkinson, R., 1996. Product formation from the reaction of the NO_3 radical with isoprene and rate constants for the reactions of methacrolein and methyl vinyl ketone with the NO_3 radical. Int. J. Chem. Kinet. 28 (12), 925–934.
Kwong, K.C., Chim, M.M., Davies, J.F., Wilson, K.R., Chan, M.N., 2018. Importance of sulfate radical anion formation and chemistry in heterogeneous OH oxidation of sodium methyl sulfate, the smallest organosulfate. Atmos. Chem. Phys. 18 (4), 2809–2820.
Lam, H.K., Kwong, K.C., Poon, H.Y., Davies, J.F., Zhang, Z., Gold, A., et al., 2019. Heterogeneous OH oxidation of isoprene-epoxydiol-derived organosulfates: kinetics, chemistry and formation of inorganic sulfate. Atmos. Chem. Phys. 19 (4), 2433–2440.
Lelieveld, J., Butler, T.M., Crowley, J.N., Dillon, T.J., Fischer, H., Ganzeveld, L., et al., 2008. Atmospheric oxidation capacity sustained by a tropical forest. Nature 452 (7188), 737–740.
Lewis, A.C., 2018. The changing face of urban air pollution. Science 359 (6377), 744–745.
Lightfoot, P.D., Cox, R.A., Crowley, J.N., Destriau, M., Hayman, G.D., Jenkin, M.E., et al., 1992. Organic peroxy-radicals-kinetics, spectroscopy and tropospheric chemistry. Atmos. Environ. A-Gen. 26 (10), 1805–1961.
Lin, V.S., Grandbois, M., McNeill, K., 2017. Fluorescent molecular probes for detection of one-electron oxidants photochemically generated by dissolved organic matter. Environ. Sci. Technol. 51 (16), 9033–9041.
Lin, Y.-H., Arashiro, M., Martin, E., Chen, Y., Zhang, Z., Sexton, K.G., et al., 2016. Isoprene-derived secondary organic aerosol induces the expression of oxidative stress response genes in human lung cells. Environ. Sci. Technol. Lett. 3 (6), 250–254.
Lin, Y.H., Zhang, Z., Docherty, K.S., Zhang, H., Budisulistiorini, S.H., Rubitschun, C.L., et al., 2012. Isoprene epoxydiols as precursors to secondary organic aerosol formation: acid-catalyzed reactive uptake studies with authentic compounds. Environ. Sci. Technol. 46 (1), 250–258.
Lin, Y.H., Zhang, H., Pye, H.O.T., Zhang, Z., Marth, W.J., Park, S., et al., 2013. Epoxide as a precursor to secondary organic aerosol formation from isoprene photooxidation in the presence of nitrogen oxides. Proc. Natl. Acad. Sci. U.S.A. 110 (17), 6718–6723.
Liu, J., D'Ambro, E.L., Lee, B.H., Lopez-Hilfiker, F.D., Zaveri, R.A., Rivera-Rios, J.C., et al., 2016. Efficient isoprene secondary organic aerosol formation from a non-IEPDX pathway. Environ. Sci. Technol. 50 (18), 9872–9880.
Liu, S., Jia, L., Xu, Y., Tsona, N.T., Ge, S., Du, L., 2017. Photooxidation of cyclohexene in the presence of SO_2: SOA yield and chemical composition. Atmos. Chem. Phys. 17 (21), 13329–13343.
Liu, Y., Brito, J., Dorris, M.R., Rivera-Rios, J.C., Seco, R., Bates, K.H., et al., 2016. Isoprene photochemistry over the Amazon rainforest. Proc. Natl. Acad. Sci. U.S.A. 113 (22), 6125–6130.
McFiggans, G., Mentel, T.F., Wildt, J., Pullinen, I., Kang, S., Kleist, E., et al., 2019. Secondary organic aerosol reduced by mixture of atmospheric vapours. Nature 565 (7741), 587–593.
Newland, M.J., Bryant, D.J., Dunmore, R.E., Bannan, T.J., Acton, W.J.F., Langford, B., et al., 2021. Low-NO atmospheric oxidation pathways in a polluted megacity. Atmos. Chem. Phys. 21 (3), 1613–1625.
Nguyen, T.B., Bates, K.H., Crounse, J.D., Schwantes, R.H., Zhang, X., Kjaergaard, H.G., et al., 2015. Mechanism of the hydroxyl radical oxidation of methacryloyl peroxynitrate (MPAN) and its pathway toward secondary organic aerosol formation in the atmosphere. Phys. Chem. Chem. Phys. 17 (27), 17914–17926.
Noziere, B., Ekstrom, S., Alsberg, T., Holmstrom, S., 2010. Radical-initiated formation of organosulfates and surfactants in atmospheric aerosols. Geophys. Res. Lett. 37, L05806.
Orlando, J.J., Tyndall, G.S., 2012. Laboratory studies of organic peroxy radical chemistry: an overview with emphasis on recent issues of atmospheric significance. Chem. Soc. Rev. 41 (19), 6294–6317.
Pathak, R.K., Stanier, C.O., Donahue, N.M., Pandis, S.N., 2007. Ozonolysis of alpha-pinene at atmospherically relevant concentrations: temperature dependence of aerosol mass fractions (yields). J. Geophys. Res. Atmos. 112 (D3), D03201.
Paulot, F., Crounse, J.D., Kjaergaard, H.G., Kuerten, A., St Clair, J.M., Seinfeld, J.H., et al., 2009. Unexpected epoxide formation in the gas-phase photooxidation of isoprene. Science 325 (5941), 730–733.
Ren, H., Sedlak, J.A., Elrod, M.J., 2021. General mechanism for sulfate radical addition to olefinic volatile organic compounds in secondary organic aerosol. Environ. Sci. Technol. 55 (3), 1456–1465.
Riva, M., Barbosa, T.D.S., Lin, Y.H., Stone, E.A., Gold, A., Surratt, J.D., 2016a. Chemical characterization of organosulfates in secondary organic aerosol derived from the photooxidation of alkanes. Atmos. Chem. Phys. 16 (17), 11001–11018.
Riva, M., Bell, D.M., Hansen, A.M.K., Drozd, G.T., Zhang, Z., Gold, A., et al., 2016b. Effect of organic coatings, humidity and aerosol acidity on multiphase chemistry of isoprene epoxydiols. Environ. Sci. Technol. 50 (11), 5580–5588.
Rudzinski, K.J., Gmachowski, L., Kuznietsova, I., 2009. Reactions of isoprene and sulphoxy radical-anions - a possible source of atmospheric organosulphites and organosulphates. Atmos. Chem. Phys. 9 (6), 2129–2140.
Ruppert, L., Becker, K.H., 2000. A product study of the OH radical-initiated oxidation of isoprene: formation of C_5-unsaturated diols. Atmos. Environ. 34 (10), 1529–1542.
Schindelka, J., Iinuma, Y., Hoffmann, D., Herrmann, H., 2013. Sulfate radical-initiated formation of isoprene-derived organosulfates in atmospheric aerosols. Faraday Discuss 165, 237–259.
Shalamzari, M.S., Kahnt, A., Vermeylen, R., Kleindienst, T.E., Lewandowski, M., Cuyckens, F., et al., 2014. Characterization of polar organosulfates in secondary organic aerosol from the green leaf volatile 3-z-hexenal. Environ. Sci. Technol. 48 (21), 12671–12678.
Shalamzari, M.S., Ryabtsova, O., Kahnt, A., Vermeylen, R., Herent, M.-F., Quetin-Leclercq, J., et al., 2013. Mass spectrometric characterization of organosulfates related to secondary organic aerosol from isoprene. Rapid Commun. Mass Spectrom. 27 (7), 784–794.
Shiraiwa, M., Ueda, K., Pozzer, A., Lammel, G., Kampf, C.J., Fushimi, A., et al., 2017. Aerosol health effects from molecular to global scales. Environ. Sci. Technol. 51 (23), 13545–13567.
Spolnik, G., Wach, P., Rudzinski, K.J., Skotak, K., Danikiewicz, W., Szmigielski, R., 2018. Improved UHPLC-MS/MS methods for analysis of isoprene-derived organosulfates. Anal. Chem. 90 (5), 3416–3423.
Stangl, C.M., Krasnomowitz, J.M., Apsokardu, M.J., Tiszenkel, L., Ouyang, Q., Lee, S., et al., 2019. Sulfur dioxide modifies aerosol particle formation and growth by ozonolysis of monoterpenes and isoprene. J. Geophys. Res. Atmos. 124 (8), 4800–4811.
Surratt, J.D., Chan, A.W.H., Eddingsaas, N.C., Chan, M., Loza, C.L., Kwan, A.J., et al., 2010. Reactive intermediates revealed in secondary organic aerosol formation from isoprene. Proc. Natl. Acad. Sci. U.S.A. 107 (15), 6640–6645.
Surratt, J.D., Murphy, S.M., Kroll, J.H., Ng, a.L.N., Hildebrandt, L., Sorooshian, A., et al., 2006. Chemical composition of secondary organic aerosol formed from the photooxidation of isoprene. J. Phys. Chem. A 110 (31), 9665–9690.
Surratt, J.D., Kroll, J.H., Kleindienst, T.E., Edney, E.O., Claeys, M., Sorooshian, A., et al., 2007. Evidence for organosulfates in secondary organic aerosol. Environ. Sci. Technol. 41 (2), 517–527.

Surratt, J.D., Gomez-Gonzalez, Y., Chan, A.W.H., Vermeylen, R., Shahgholi, M., Kleindienst, T.E., et al., 2008. Organosulfate formation in biogenic secondary organic aerosol. J. Phys. Chem. A 112 (36), 8345–8378.

Szmigielski, R., 2016. Evidence for C_5 organosulfur secondary organic aerosol components from in-cloud processing of isoprene: role of reactive SO_4 and SO_3 radicals. Atmos. Environ. 130, 14–22.

Vereecken, L., Harder, H., Novelli, A., 2012. The reaction of Criegee intermediates with NO, RO_2, and SO_2, and their fate in the atmosphere. Phys. Chem. Chem. Phys. 14 (42), 14682–14695.

Wach, P., Spolnik, G., Surratt, J.D., Blaziak, K., Rudzinski, K.J., Lin, Y.-H., et al., 2020. Structural characterization of lactone-containing MW 212 organosulfates originating from isoprene oxidation in ambient fine aerosol. Environ. Sci. Technol. 54 (3), 1415–1424.

Wang, C., Tian, C.-Y., Zhao, Y., Jiang, S., Wang, T., Zheng, H., et al., 2023. Observation of confinement-free neutral group three transition metal carbonyls $Sc(CO)_7$ and $TM(CO)_8$ (TM=Y, La). Angew. Chem., Int. Ed. 62, e202305490.

Wang, C., Fu, L., Yang, S., Zheng, H., Wang, T., Gao, J., et al., 2022. Infrared spectroscopy of stepwise hydration motifs of sulfur dioxide. J. Phys. Chem. Lett. 13 (24), 5654–5659.

Weber, R.J., Marti, J.J., McMurry, P.H., Eisele, F.L., Tanner, D.J., Jefferson, A., 1996. Measured atmospheric new particle formation rates: implications for nucleation mechanisms. Chem. Eng. Commun. 151, 53–64.

Wennberg, P.O., Bates, K.H., Crounse, J.D., Dodson, L.G., McVay, R.C., Mertens, L.A., et al., 2018. Gas-phase reactions of isoprene and its major oxidation products. Chem. Rev. 118 (7), 3337–3390.

Xu, L., Guo, H., Boyd, C.M., Klein, M., Bougiatioti, A., Cerully, K.M., et al., 2015. Effects of anthropogenic emissions on aerosol formation from isoprene and monoterpenes in the southeastern United States. Proc. Natl. Acad. Sci. U.S.A. 112 (1), 37–42.

Yang, Z., Li, K., Tsona, N.T., Luo, X., Du, L., 2023. SO_2 enhances aerosol formation from anthropogenic volatile organic compound ozonolysis by producing sulfur-containing compounds. Atmos. Chem. Phys. 23 (1), 417–430.

Yao, M., Zhao, Y., Hu, M., Huang, D., Wang, Y., Yu, J.Z., et al., 2019. Multiphase reactions between secondary organic aerosol and sulfur dioxide: kinetics and contributions to sulfate formation and aerosol aging. Environ. Sci. Technol. Lett. 6 (12), 768–774.

Ye, J., Abbatt, J.P.D., Chan, A.W.H., 2018. Novel pathway of SO_2 oxidation in the atmosphere: reactions with monoterpene ozonolysis intermediates and secondary organic aerosol. Atmos. Chem. Phys. 18 (8), 5549–5565.

Zang, X., Zhang, Z., Jiang, S., Zhao, Y., Wang, T., Wang, C., et al., 2022. Aerosol mass spectrometry of neutral species based on a tunable vacuum ultraviolet free electron laser. Phys. Chem. Chem. Phys. 24 (27), 16484–16492.

Zhang, B., Yu, Y., Zhang, Y.-Y., Jiang, S., Li, Q., Hu, H.-S., et al., 2020. Infrared spectroscopy of neutral water clusters at finite temperature: evidence for a noncyclic pentamer. Proc. Natl. Acad. Sci. U.S.A. 117 (27), 15423–15428.

Zhang, D., Zhang, R.Y., 2002. Mechanism of OH formation from ozonolysis of isoprene: a quantum-chemical study. J. Am. Chem. Soc. 124 (11), 2692–2703.

Zhang, H., Worton, D.R., Lewandowski, M., Ortega, J., Rubitschun, C.L., Park, J.-H., et al., 2012. Organosulfates as tracers for secondary organic aerosol (SOA) formation from 2-methyl-3-buten-2-ol (MBO) in the atmosphere. Environ. Sci. Technol. 46 (17), 9437–9446.

Zhao, D., Pullinen, I., Fuchs, H., Schrade, S., Wu, R., Acir, I.-H., et al., 2021. Highly oxygenated organic molecule (HOM) formation in the isoprene oxidation by NO_3 radical. Atmos. Chem. Phys. 21 (12), 9681–9704.